



1 **Why do GCMs overestimate the aerosol cloud lifetime effect? A comparison of CAM5**
2 **and a CRM**

3 **Cheng Zhou¹, Joyce E. Penner¹**

4 (1){University of Michigan, Ann Arbor, MI, USA}

5

6 Corresponding author: C. Zhou (zhouc@umich.edu).

7

8

9 **Abstract**

10 Observation-based studies have shown that the aerosol cloud lifetime effect or the
11 increase of cloud liquid water (LWP) with increased aerosol loading may have been
12 overestimated in climate models. Here, we simulate shallow warm clouds on 05/27/2011 at
13 the Southern Great Plains (SGP) measurement site established by Department of Energy's
14 Atmospheric Radiation Measurement (ARM) Program using a single column version of a
15 global climate model (CAM5.3) and a cloud resolving model (CRM). The LWP simulated by
16 CAM increases substantially with aerosol loading while that in the CRM does not. The
17 increase of LWP in CAM is caused by a large decrease of the autoconversion rate when cloud
18 droplet number increases. In the CRM, the autoconversion rate is also reduced, but this is
19 offset or even outweighed by the increased evaporation of cloud droplets near cloud top,
20 resulting in an overall decrease in LWP. Our results suggest that climate models need to
21 include the dependence of cloud top growth and the evaporation/condensation process on
22 cloud droplet number concentrations.

23

24 **1. Introduction**

25 Traditionally aerosols have been thought to lengthen cloud lifetime (Albrecht, 1989) by
26 increasing droplet number and reducing droplet size thereby delaying and reducing the
27 formation of rain in clouds. These longer lived clouds would then increase cloud cover and
28 reflect more sunlight. Yet observational evidence for these lifetime effects is limited and
29 contradictory (Boucher et al. 2013). Observations of ship tracks show that marine boundary-
30 layer clouds polluted by aerosol particles show that the liquid water path (LWP) can either
31 increase or decrease depending on factors like mesoscale cloud cellular structures, dryness of
32 the free troposphere and boundary layer depth (Christensen and Stephens 2011; Chen et al.,
33 2012, 2015). Results from large-eddy simulations (LES) and cloud resolving models (CRM)



34 show the response of cloud water to aerosols is complicated by competing effects like
35 reduced precipitation formation efficiency in clouds and enhanced evaporation at cloud top or
36 in the downdraft regions of cloud edges (Ackerman et al. 2004; Xue and Feingold, 2006; Tao
37 et al., 2012). Since CRMs and LES models resolve clouds, have more complete physics and
38 depend less on subgrid parameterizations than general circulations models (GCMs), they are
39 often used together with field measurements to evaluate and improve parameterizations of
40 clouds and radiation used in climate models. Several previous studies have compared single
41 column models, which are essentially an isolated column of a GCM, and cloud resolving
42 models (Moncreiff et al. 1997; Ghan et al., 2000; Xu et al., 2002; Xie et al., 2002; Xie et al.,
43 2005). Lee and Penner (2010) extended these types of comparisons to the response of the two
44 models (CAM and a CRM) to increases in aerosols in marine stratocumulus. Both models
45 found that LWP increased but the effect from increased condensation dominated in the CRM
46 while the effect from decreased autoconversion dominated in CAM. Wang et al. (2012) used
47 satellite observations of the precipitation frequency susceptibility together with model
48 simulations to constrain cloud lifetime effects in GCMs. They show that GCMs tend to
49 overestimate the precipitation frequency susceptibility of marine clouds. Since the LWP
50 increase as a result of increased cloud condensation nuclei concentrations is highly correlated
51 with precipitation frequency susceptibility in climate models, they surmise that the LWP
52 increase is too high and show that this overestimation could be “fixed” by reducing the
53 dependence of the autoconversion rate on cloud droplet number in the models.

54 In this study, we simulated continental shallow warm clouds observed on 05/27/2011 at
55 the Southern Great Plains (SGP) measurement site established by Department of Energy's
56 Atmospheric Radiation Measurement (ARM) Program using the single column version of a
57 global climate model (CAM5.3) and a cloud resolving model and explored plausible causes
58 for the differences in the response of these two models to increases in aerosols. Here we
59 specifically identify that the cloud top growth and turbulence mixing parameterizations
60 within CAM require improvement, rather than only the autoconversion rate. Section 2
61 describes the models and set-up. Section 3 presents results followed by conclusions and a
62 discussion in section 4.

63

64 **2. Description of models and set-up**

65 We used the Goddard Cumulus Ensemble model (GCE) with recent improvements (Tao
66 et al. 2014) and the single column version of Community Atmosphere Model (CAM, version
67 5.3) which is the atmospheric component of the Community Earth System Model (CESM,



68 version 1.2.2). Readers are referred to Neale et al. (2012) for more model details of CAM.
69 Here we briefly summarize the two most critical parameterizations for warm stratus clouds in
70 CAM: cloud microphysics and cloud macrophysics. The cloud microphysics (version MG1.5)
71 is a two-moment scheme (Morrison et al. 2005, Morrison and Gettelman 2008) which
72 predicts the number concentrations and mixing ratios of cloud droplets. The source term for
73 the cloud droplets in warm clouds only includes the activation of cloud condensation nuclei
74 while the sink terms include the instantaneous evaporation of falling cloud droplets into the
75 clear portions of grids beneath clouds, autoconversion of cloud droplets to form rain, and
76 accretion of cloud droplets by rain. The first two sink terms (instantaneous evaporation of
77 falling cloud droplets and autoconversion) depend on the aerosol number concentration since
78 the terminal falling speed of cloud droplets is related to cloud droplet size and the
79 autoconversion rate is inversely proportional to cloud droplet number ($\sim N_c^{-1.79}$ where N_c is
80 the in-cloud cloud droplet number). The last sink term (accretion) does not depend on the
81 cloud droplet number (Khairoutdinov and Kogan 2000). The conversion of water vapor to
82 cloud condensate is computed by the cloud macrophysics parameterization which also
83 predicts the cloud fraction in each grid as well as the horizontal and vertical overlapping
84 structures of clouds. Following Smith (1990), the liquid fraction of stratus clouds in CAM5 is
85 derived from an assumed triangular distribution of total relative humidity (i.e. the sum of
86 water vapor and liquid cloud water). The net conversion rate of water vapor to stratus
87 condensate is diagnosed using saturation equilibrium conditions: (1) the RH over the water
88 within the liquid stratus is always 100%, and (2) no liquid stratus droplets exist in the clear
89 portion of the grid.

90 The Goddard Cumulus Ensemble model (GCE) is a CRM that has been developed and
91 improved at the NASA Goddard Space Flight Center (GSFC). Its development and main
92 features were published in Tao and Simpson (1993) and Tao et al. (2003) and recent
93 improvements and applications were presented in (Tao et al. 2014). The GCE model used in
94 the present paper uses the double moment version of the Colorado State University Regional
95 Atmospheric Modeling System (RAMS) bulk microphysics scheme (Saleeby and Cotton,
96 2004) which assumes a gamma-shaped particle size distribution for three species of liquid
97 (small and large cloud droplets and rain). The small cloud droplets range from 2 to 40
98 microns in diameter, and the large cloud droplets range from 40 to 80 microns. Collection of
99 cloud droplets is simulated using stochastic collection equation solutions, facilitated by bin-



100 emulating look-up tables. Readers are referred to Lee et al. (2009) and Tao et al. (2014) for
101 more detailed descriptions of the model physics.

102 CAM has 30 vertical layers and a variable vertical resolution which depends on the
103 surface pressure and the vertical temperature profile. In the case studied in this paper the
104 vertical resolution is roughly 100 meters near the surface and stretches to about 300 m at 2
105 km decreasing to 1 km at 10 km. The time step is 20 minutes. GCE has 128 grids in the two
106 horizontal directions and 144 vertical layers. The horizontal resolution is 50 m, so the domain
107 size is 6.4 km \times 6.4 km. GCE also uses a stretched vertical resolution that varies from about
108 30 m near the surface to about 90 m at 2 km and further to \sim 200 m at 10 km. The time step of
109 the GCE model is 1 second. Both models use the same initial conditions (surface
110 pressure/temperature, vertical temperature/water vapor/wind profiles), boundary conditions
111 (surface sensible/latent heat fluxes, surface pressure/temperature). Advective tendencies of
112 temperature and moisture (both vertically and horizontally) are specified based on an
113 objective variational analysis approach (Xie et al. 2014) fit to the Midlatitude Continental
114 Convective Clouds Experiment (MC3E) campaign observations which were conducted from
115 April to June 2011 near the DOE ARM Southern Great Plains (SGP) site. The analyzed
116 advective tendencies cover the period from April 22nd to June 21th, 2011. Middle to deep
117 convective clouds were observed in most cloudy days. For this study, May 27th, 2011, was
118 selected because middle and high clouds were absent during a low cloud period observed
119 near noon. The vertical wind/temperature/moisture/cloud fraction profiles, surface
120 latent/sensible heat fluxes, and advective tendencies of temperature and moisture are shown
121 in Fig S1. Low clouds occurred from \sim 1 km to \sim 2 km near the top of the boundary layer and
122 were strongly modulated by the advective tendencies of temperature and moisture. Positive
123 moisture flux and negative temperature flux were observed during the growing stage of the
124 clouds while negative moisture flux and positive temperature flux were observed during the
125 decaying stage. Both models are initialized at 00:00 local time and run for 18 hours.

126 To study the effect of aerosols on clouds, we scaled the aerosol vertical profiles in both
127 models by increasing the surface aerosol number concentrations from 250 cm⁻³ to 4000 cm⁻³.
128 GCE uses a prescribed aerosol profile which decreases linearly from its surface concentration
129 to 100 cm⁻³ at an altitude of 14 km and above. The activation of aerosols to cloud droplets is
130 based on the grid resolved vertical updraft velocity, temperature, and aerosol number and size
131 from a look-up table constructed from results of a Lagrangian parcel model (Saleeby and
132 Cotton, 2004). For CAM, we extracted the averaged aerosol profile in May at this location
133 from a 5-year run of CAM5 using the MAM3 aerosol module and scaled the aerosol profile



134 based on the surface aerosol number concentrations (see Fig. S2 for profiles of aerosol
135 number concentrations used in the two models). The activation of aerosols into cloud droplets
136 in CAM is diagnosed as a function of the modeled subgrid-scale updraft velocity and aerosol
137 compositions/sizes/numbers (Abdul-Razzak and Ghan 2000). Even though we set the total
138 surface aerosol number concentrations the same in the two models, the aerosol composition,
139 size, and number at cloud level, and the nucleation schemes are inherently different. However,
140 since this paper focuses on a sensitivity study which is aimed at revealing the different cloud
141 physical representations in the two models that lead to *opposite* responses of the simulated
142 LWP to increasing aerosol number concentrations that cover a wide range (250 cm^{-3} to 4000
143 cm^{-3}) rather than quantifying the changes of the LWP, these differences are not critical to the
144 conclusions of the paper. To better isolate differences in the aerosol indirect effect in the two
145 models, we also turned off the aerosol direct radiative effect.

146

147 **3. Results**

148 Figure 1a shows the observed cloud fractions from the early morning to the late afternoon
149 on May 27th, 2011 at the SGP site, while Figures 1b and 1c show the simulated mean cloud
150 water content from the two models assuming a surface aerosol number concentration of 500
151 cm^{-3} . Compared to the observations, the simulated clouds from both models begin later in the
152 day and have a smaller vertical coverage. But the models compare relatively well to each
153 other which suggests that differences between the models and the observations may largely
154 be caused by the possible errors/uncertainties associated with the derived initial conditions or
155 advective tendencies. Nevertheless, we can see that the GCE model captures the observed
156 growth of the clouds with height while CAM does not. A detailed analysis of the GCE (next
157 paragraph) shows that the clouds could be loosely classified as stratocumulus which occur
158 near the top of the planetary boundary layer (PBL) and are mainly driven by long wave
159 radiative cooling offset by short wave radiative heating. This is corroborated by CAM's
160 result which shows all simulated clouds are stratus clouds and no convective clouds are able
161 to form above the PBL. The advective tendencies of heat and moisture also strongly modulate
162 the clouds. For example, the positive moisture tendency before 14:00 hours leads to slightly
163 larger in-cloud water vapor mixing ratio than that below the clouds (more details will be
164 presented in the discussion of Figure 2). Figure 1d and 1e show the domain averaged liquid
165 water path (LWP) from the two models for five different surface aerosol number
166 concentrations (250 , 500 , 1000 , 2000 and 4000 cm^{-3}). Both models underestimate the LWP
167 during the day, similar to their underestimation of cloud cover. GCE shows relatively small



168 changes in the LWP when using different surface aerosol numbers. The LWP slightly
169 increases with the increasing aerosol number before ~14:00 but starts to decrease with the
170 increasing aerosol number when the clouds start to decay after around 14:00. On the other
171 hand, the LWP from CAM increases substantially and consistently with increasing aerosol
172 number and matches the observed LWP better when the surface aerosol number is equal to
173 4000 cm^{-3} . As noted earlier, due to uncertainties associated with the derived forcing data as
174 well as uncertainties in the models, this should not be interpreted as proof that CAM
175 represents the physics better. Figure 1f and 1g show the precipitation rates from the two
176 models. The precipitation rate from CAM consistently decreases with increasing aerosol
177 number and is nearly suppressed after 13:00. The change is most prominent when the aerosol
178 number is increased from 250 to 500 cm^{-3} . The precipitation rates from GCE are overall very
179 small with maximum values less than 0.08 mm day^{-1} . The change in precipitation for GCE
180 with increasing aerosol numbers is a little more complex. During the growing phase of the
181 clouds, as in CAM, the precipitation rate decreases. But during the decaying phase, the
182 precipitation rate actually increases even though the LWP decreases.

183 Figures 2a-2c show the domain averaged potential temperatures (θ), total water specific
184 humidity (q_t) and cloud water content (q_c) at three times (13:00, 14:00 and 15:00) from the
185 case with surface aerosol numbers equal to 250 cm^{-3} (dash-dotted curves) and 1000 cm^{-3}
186 (solid curves), respectively. q_t is the sum of q_c , rain and water vapor mixing ratios, which is
187 an invariant within the PBL for stable non-precipitating well-mixed stratocumulus. θ and q_t
188 from the two cases almost overlap except near the cloud top at 14:00 and 15:00. Fig. 2a
189 shows the growth of the PBL. At 13:00 the clouds do not completely reside within the PBL as
190 the top of the PBL is at about 1.2 km which is lower than the cloud top height (~1.5 km)
191 shown in Fig. 2c. Fig. 2b shows that q_t in the top half of the cloud (from ~1.2-1.5 km) is
192 larger than q_t in the bottom half of clouds (from ~1-1.2 km) and q_t below the clouds at 13:00.
193 This suggests that the top half of the clouds are not fully coupled with the surface and the
194 cloud water in the top half of the clouds is strongly affected by the horizontally advected
195 positive moisture flux. At 14:00 and 15:00, the advected moisture flux becomes negative and
196 the PBL is high enough that the clouds reside fully within the top of the PBL and possess the
197 characteristics of well-mixed stratocumulus. The domain averaged long-wave cooling rate at
198 the cloud top height is about 2 K hr^{-1} and is offset by a short-wave heating of about 0.5 K hr^{-1} .
199 Fig. 2c shows that the cloud top is a little higher for the higher aerosol case, but the maximum
200 values of q_c are smaller. A closer look at θ in Fig 2a also shows that the top of the PBL which



201 is near 1.5 km is higher and colder in the higher aerosol number case. These differences of
202 q_c and θ between the two cases are clearer in an enlarged portion of Fig 2a and 2b shown in
203 Fig. S3. The potential temperature in the sub-cloud layer at 14:00 and 15:00 is also slightly
204 higher (about 0.005 K) for higher aerosols. Figs. 2d to 2i show the time-averaged profiles of
205 q_c and the net result of condensation and evaporation (Conden-Evap) during two 1-hour
206 intervals (Fig. 2d-f for 13:00 to 14:00 and Fig. 2g-i for 14:00 to 15:00) representing the
207 growing and decaying phases of the cloud, respectively. Figures 2e and 2h show that a net
208 evaporation occurs just below the cloud base and near the cloud top. The largest net
209 condensation is located near the cloud base. The most obvious change between the growing
210 phase and decaying phase of the cloud is the increased evaporation near the cloud top,
211 especially for the high aerosol number case (see the changes from blue curve to the red curve
212 at around 1.5 km from Fig. 2e and Fig. 2h). Choosing $(\text{Conden} - \text{Evap})/q_c$ as a measure
213 of the inverse of the characteristic evaporation time of cloud droplets, Figures 2f and 2i show
214 that it increases substantially from 300 hr^{-1} to about 600 hr^{-1} (an evaporation time of ~ 6
215 seconds) near the cloud top for the higher aerosol number case.

216 Figure 3 shows the LWP and the column integrated LWP source and sink terms from the
217 low and high aerosol cases (250 and 1000 cm^{-3}). The source term for LWP only includes the
218 net condensation term (Conden – Evap) while the loss terms include autoconversion and
219 accretion. Since CAM includes a separate autoconversion and accretion terms while GCE
220 does not, we combined autoconversion and accretion as one term (Auto+Accre) for easier
221 comparison. As shown in Fig. 1, when we increase the aerosol numbers from 250 to 1000 cm^{-3} ,
222 the LWP increase is relatively small in GCE and substantially larger in CAM. Both models
223 show decreased Auto+Accre which acts to increase the LWP. This is expected as increased
224 aerosol numbers increase the cloud droplet number which decreases the autoconversion rate.
225 But CAM shows much larger changes, especially before 13:00 hours. This is likely due to the
226 fact that the two models use different cloud droplet activation schemes as well as schemes to
227 parameterize the autoconversion and accretion processes. Moreover, in GCE, the decreased
228 autoconversion is largely offset or even outweighed by increased evaporation. As shown in
229 Fig. 2e and 2h the increased evaporation occurs near cloud top. The increased evaporation
230 near the cloud top and the higher PBL suggests that higher aerosol number concentrations
231 lead to smaller cloud droplet sizes and enhanced evaporation at the cloud top which can then
232 decrease the temperature slope near the cloud top and promote the sinking of entrained air
233 into the cloud layer, a point made previously by Bretherton et al. (2007). This evaporation-



234 entrainment feedback mechanism was also observed in small cumulus clouds (Small et al.
235 2009). Before ~14:00, the effect from the decreased autoconversion rates outweighs the
236 effect from increased evaporation so that the LWP shows a slight increase. But as the cloud
237 starts to decay after ~14:00, the PBL keeps growing and the enhanced
238 evaporation/entrainment rates accelerate the decaying process. Thus the LWP decreases
239 faster and eventually a smaller LWP results over the decaying period for the high aerosol
240 case. In the CAM model, the change of the net condensation term (Conden – Evap) is smaller
241 than that in the CRM model. Since the simulated cloud top remains unchanged between
242 12:00 and 15:00 hours, the drying effect seen in the CRM due to enhanced entrainment of
243 overlying dry air is not present. This is likely due to the fact that the moist turbulence scheme
244 in CAM does not depend on the cloud droplet number/size and the condensation and
245 evaporation in the CAM's macrophysics scheme is not linked to the cloud droplet number or
246 size. Even though the instantaneous evaporation of falling cloud droplets into the clear
247 portions of grids beneath clouds in the microphysics scheme is related to the cloud droplet
248 number, it is about one order of magnitude smaller than the net condensation term in the
249 macrophysics scheme. Consequently the net condensation and evaporation is less sensitive to
250 the change in aerosol number and the effect from the decreased autoconversion rate
251 dominates the condensate loss, leading to an increase of the LWP.

252 To confirm that the effect from enhanced entrainment at the cloud top is the critical
253 reason for the reduced LWP change in GCE, we ran a sensitivity test to reduce the cloud top
254 mixing by increasing the grid spacing from 50 m to 100 km. With this larger grid spacing, we
255 greatly reduced the overshooting at the cloud top by reducing the maximum vertical speed in
256 the updrafts from meters per second to a few centimeters per second. As a result, the
257 enhanced entrainment effect was reduced and the microphysical effect from the reduced
258 autoconversion rate dominated. Figure 4 shows that the LWP from GCE decreases by about
259 5% for the $dx=50$ m case while it increases by about 12% for the $dx=100$ km case when the
260 surface aerosol number is increased from 250 cm^{-3} to 4000 cm^{-3} . We also ran two more tests
261 to explore whether the LWP sensitivity in CAM could match that in the GCE. In the default
262 set-up of CAM, the autoconversion rate is inversely proportional to cloud droplet number
263 ($\sim N_c^{-1.79}$ where N_c is the in-cloud cloud droplet number). We ran two cases, auto06 and
264 auto00, each with a reduced dependence of the autoconversion rate on the cloud droplet
265 number. In case auto06, the autoconversion rate is proportional to $N_c^{-0.60}$ and in case auto00,
266 the autoconversion rate does not depend on the cloud droplet number. The autoconversion



267 rate is scaled in both cases to produce the same rate as that from the default case at a droplet
268 number concentration of 100 cm^{-3} . As shown in Fig. 4, the LWP from the default case is
269 more than doubled when the surface aerosol number is increased from 250 cm^{-3} to 4000 cm^{-3}
270 while the LWP from auto06 only increases by ~50% and the LWP from case auto00 remains
271 almost unchanged. These results suggest that the dependence of the autoconversion rate on
272 the cloud droplet number can play a determining role on the simulated LWP consistent with
273 the findings of precipitation frequency susceptibility in Wang et al. (2012). However, this
274 adjustment is unable to simulate decreases in LWP seen in the GCE model.

275

276 4. Conclusion and Discussion

277 We simulated shallow warm clouds on May 27th, 2011 at the DOE ARM SGP site with a
278 cloud resolving model (Goddard Cumulus Ensemble model) and a single column model
279 (CAM) using the same initial/boundary conditions and advected moisture/heat tendencies
280 derived from the MC3E campaign data. The liquid water path (LWP) simulated by CAM
281 shows a large dependence on the aerosol loading and is more than doubled when the surface
282 aerosol number is increased from 250 cm^{-3} to 4000 cm^{-3} while the LWP simulated by the
283 CRM decreases by ~5%. The high sensitivity of LWP on aerosol loading in CAM can be
284 reduced by reducing the dependence of the autoconversion rate on the cloud droplet number
285 concentration, but is unable to reproduce the decrease in LWP seen in the CRM. Whereas
286 Wang et al. (2012) concluded that this term in GCM models can be tuned to fit observations
287 of the precipitation frequency susceptibility, we find that the poor representation of
288 entrainment and droplet evaporation in CAM model may be the fundamental cause of
289 differences with the more complete CRM. While in the CRM a reduced autoconversion rate
290 is also observed with increased aerosol loading, it is offset or even outweighed by the
291 increased evaporation of cloud droplets near the cloud top. The increased evaporation cools
292 the cloud top, reduces the temperature lapse rate and thus increases the entrainment of drier
293 air above the cloud top and accelerates the decaying process of the clouds. Reduced LWP
294 through enhanced entrainment with increased aerosol number has also been reported in
295 previous literature using large eddy simulations (e.g., Ackerman 2004, Bretherton et al. 2007,
296 Seifert et al. 2015). One unique aspect of the present paper is that the response of the LWP
297 over the lifetime of the cloud is negative in the CRM while it is positive in the CAM model
298 for the same forcing conditions. One critical deficiency of CAM for this case is that the effect
299 from increased mixing of drier air from above the cloud layer through enhanced entrainment
300 caused by increased aerosol numbers is missing. First, CAM is not able to simulate the



301 growth of the cloud top due to its coarse vertical resolution. However, even if the CAM
302 vertical resolution were high enough to capture the growth of the cloud top, since the moist
303 turbulence scheme and the evaporation of cloud condensate in the cloud macrophysics
304 parameterization at the cloud top are not related to the cloud droplet number, aerosol number
305 will not have a direct impact on the cloud top mixing or the LWP.

306 Our CRM model results demonstrate that the relative importance of the decreased
307 autoconversion rate effect and the enhanced entrainment effect from increased aerosol
308 numbers can change based on environmental conditions as manifested in different stages
309 during the cloud lifecycle. Thus, one may need to distinguish the cloud stage when studying
310 the aerosol lifetime effect either with a model or from observations.

311

312 **5. Acknowledgements**

313 This work was supported by the DOE under grant #DOE DE-SC0008486. We thank
314 Derek Posselt and S.-S. Lee for helpful discussions and setting up the GCE model. We also
315 thank Shaocheng Xie for providing the ARM forcing data. We acknowledge high-
316 performance computing support from National Energy Research Scientific Computing Center
317 (NERSC).

318

319 **References**

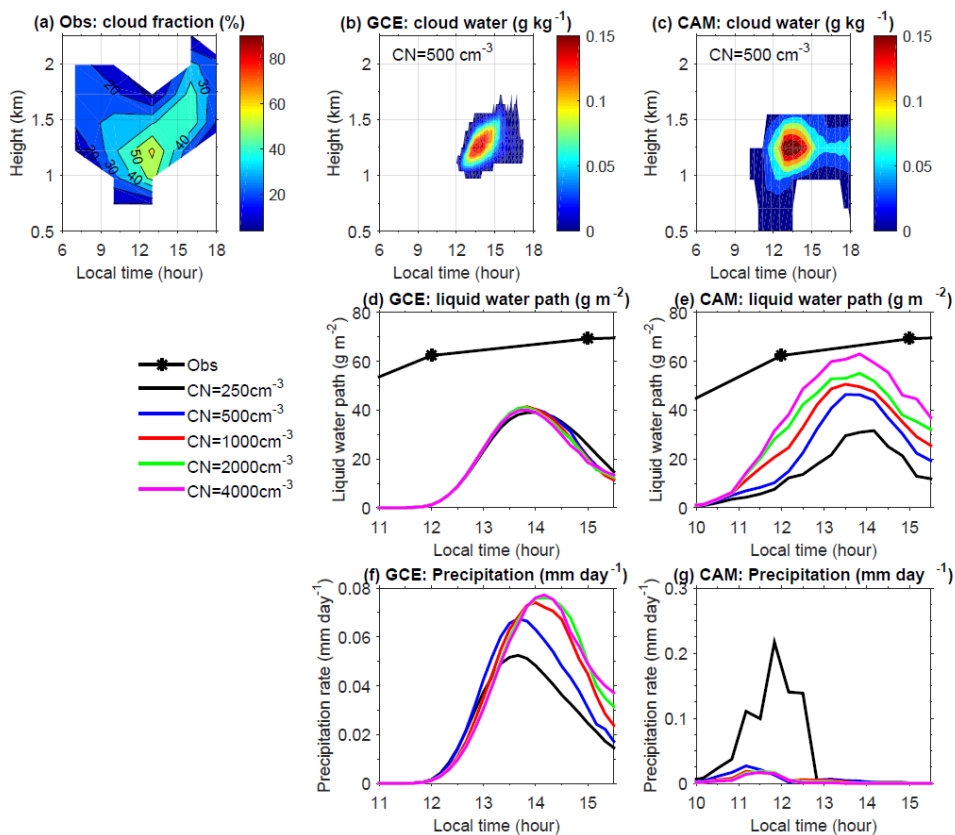
- 320 Abdul-Razzak, H. and Ghan, S.: A parameterisation of aerosol activation 2. Multiple aerosol
321 types, *J. Geophys. Res.*, 105, 6837–6844, 2000.
- 322 Boucher, O., et al.: Clouds and aerosols, in *Climate Change 2013: The Physical Science*
323 *Basis. Contribution of Working Group I to the Fifth Assessment Report of the*
324 *Intergovernmental Panel on Climate Change*, edited by T. Stocker, et al., Cambridge
325 Univ. Press, Cambridge, U. K., 2013.
- 326 Bretherton, C. S., Blossey, P.N. and Uchida J.: Cloud droplet sedimentation, entrainment
327 efficiency, and subtropical stratocumulus albedo, *Geophys. Res. Lett.*, 34, L03813,
328 doi:10.1029/2006GL027648, 2007.
- 329 Chen, Y.-C., Christensen, M. W., Diner, D. J. and Garay, M. J.: Aerosol-cloudinteractions in
330 ship tracks using TerraMODIS/MISR, *J. Geophys. Res. Atmos.*, 120,2819–2833,
331 doi:10.1002/2014JD022736, 2015.
- 332 Chen, Y.-C., Christensen, M. W., Xue, L., Sorooshian, A., Stephens, G. L., Rasmussen, R.
333 M. and Seinfeld, J. H.: Occurrence of lower cloud albedo in ship tracks, *Atmos. Chem.*
334 *Phys.*, 12, 8223–8235, 2012.



- 335 Christensen, M. W. and Stephens, G. L.: Microphysical and macrophysical responses of
336 marine stratocumulus polluted by underlying ships: Evidence of cloud deepening, J.
337 Geophys. Res., 116, D03201, doi:10.1029/2010JD014638, 2011.
- 338 Ghan, S., Randall, D., Xu, K.-M., Cederwall, R., Cripe, D., Hack, J., Iacobellis, S., Klein, S.,
339 Krueger, S., Lohmann, U., Pedretti, J., Robock, A., Rotstayn, L., Somerville, R.,
340 Stenchikov, G., Sud, Y., Walker, G., Xie, S., Yio, J., and Zhang, M.: A comparison of
341 single column model simulations of summertime midlatitude continental convection, J.
342 Geophys. Res., 105, 2091–2124, 2000
- 343 Khairoutdinov, M. F. and Y. Kogan, A new cloud physics parameterization in a large-eddy
344 simulation model of marine stratocumulus, Mon. Weather Rev., 128, 229–243, 2000.
- 345 Lee, S. S. and Penner, J. E.: Comparison of a global-climate model to a cloud-system
346 resolving model for the long-term response of thin stratocumulus clouds to preindustrial
347 and present-day aerosol conditions, Atmos. Chem. Phys., 10, 6371–6389,
348 doi:10.5194/acp-10-6371-2010, 2010.
- 349 Lee, S. S., Penner, J. E. and Saleeby, S. M.: Aerosol effects on liquid-water path of thin
350 stratocumulus clouds, J. Geophys. Res., 114, D07204, doi:10.1029/2008JD010513,
351 2009.
- 352 Moncrieff, M. W., Krueger, S. K., Gregory, D., Redelsperger, J.-L. and Tao, W.-K.: GEWEX
353 Cloud System Study (GCSS) Working Group 4: Precipitating convective systems, Bull.
354 Am. Meteorol. Soc., 78, 831–845, 1997.
- 355 Morrison, H., and Gettelman, A.: A new two-moment bulk stratiform cloud microphysics
356 scheme in the NCAR Community Atmosphere Model (CAM3), Part I: Description and
357 numerical tests, J. Clim., 21 (15), 3642–3659, 2008.
- 358 Morrison, H., Curry, J. A. and Khvorostyanov, V. I.: A new double-moment microphysics
359 parameterization for application in cloud and climate models. part i: Description, J.
360 Atmos. Sci., 62, 1665–1677, 2005.
- 361 Saleeby S. M. and Cotton, W. R.: A large droplet mode and prognostic number concentration
362 of cloud droplets in the Colorado State University Regional Atmospheric Modeling
363 System (RAMS). Part I: Module descriptions and supercell test simulations. J. Appl.
364 Meteor., 43, 182–195, 2004.
- 365 Seifert, A., Heus, T., Pincus, R., and Stevens, B.: Large-eddy simulation of the transient and
366 near-equilibrium behavior of precipitating shallow convection, J. Adv. Model. Earth
367 Syst., 7, 1918–1937, doi:10.1002/2015MS000489, 2015.
- 368 Small, J. D., Chuang, P. Y., Feingold, G. and Jiang, H.: Can aerosol decrease cloud lifetime?,

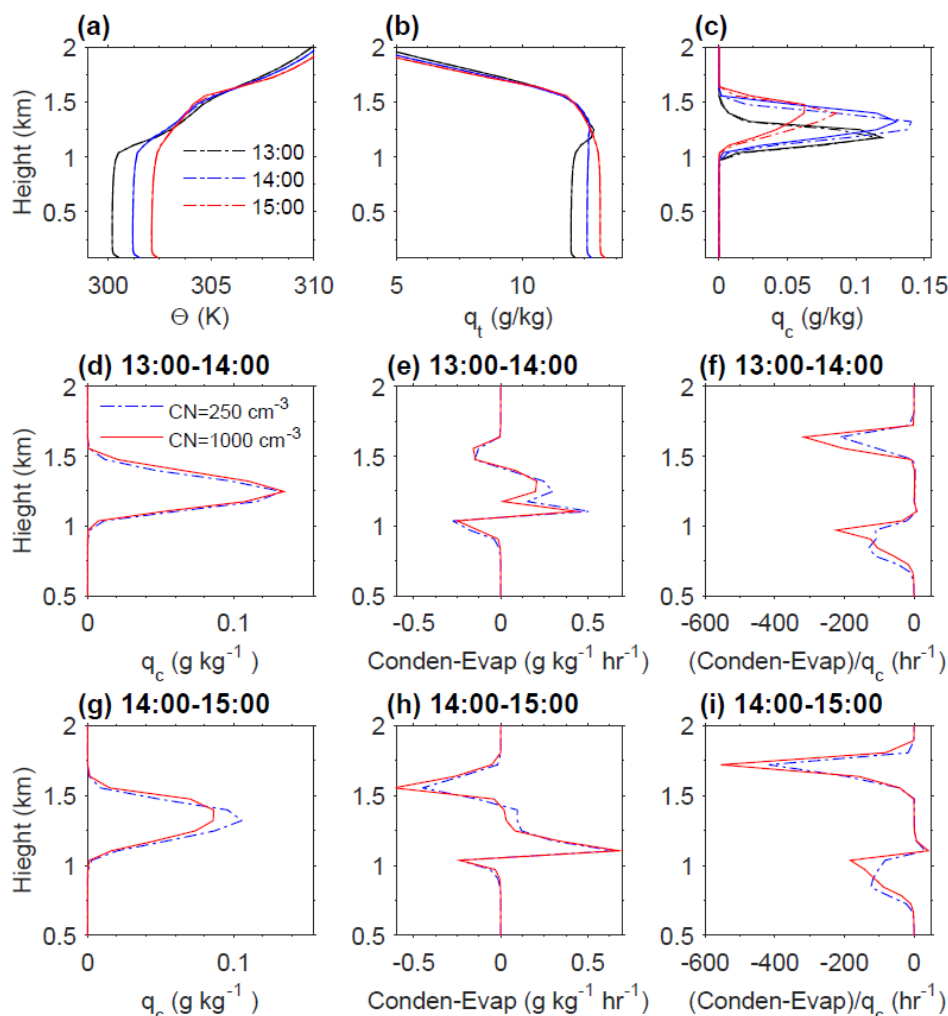


- 369 Geophys. Res. Lett., 36, L16806, doi:10.1029/2009GL038888, 2009.
- 370 Smith, R. N. B.: A scheme for predicting layer clouds and their water content in a general
371 circulation model, Q. J. R. Meteorol. Soc., 116, 435–460, 1990.
- 372 Tao, W.-K.: Goddard Cumulus Ensemble (GCE) model: application for understanding
373 precipitation processes. AMS Meteorological Monographs— Cloud Systems,
374 Hurricanes and TRMM 107–138, 2003.
- 375 Tao, W.-K., Lang, S., Zeng, X.P., Li, X.W., Matsui, T., Mohr, K., Posselt, D., Chern, J.,
376 Peters-Lidard, C., Norris, P.M., Kang, I.S., Choi, I., Hou, A., Lau, K.-M. and Yang, Y.-
377 M.: The Goddard Cumulus Ensemble model (GCE): Improvements and applications for
378 studying precipitation processes, Atmos. Res., 143, 392–424, 2014.
- 379 Tao, W.-K. and Simpson, J.: The Goddard Cumulus Ensemble Model. Part I: model
380 description. Terr. Atmos. Ocean. Sci. 4, 35–72, 1993.
- 381 Wang, M., Ghan, S., Liu, X., L'Ecuyer, T. S., Zhang, K., Morrison, H., Ovchinnikov, M.,
382 Easter, R., Marchand, R., Chand, D., Qian, Y., Penner, J.E.: Constraining cloud lifetime
383 effects of aerosols using A-Train satellite observations, Geophys. Res. Lett., 39, L15709,
384 doi:10.1029/2012GL052204, 2012.
- 385 Xie, S, Xu, K.-M., Cederwall, R. T., Bechtold, P., Genio, A. D. D., Klein, S. A., Cripe, D. G.,
386 Ghan, S. J., Gregory, D., Iacobellis, S. F., Krueger, S. K., Lohmann, U., Petch, J. C.,
387 Randall, D. A., et al.: Intercomparison and evaluation of cumulus parametrizations
388 under summertime midlatitude continental conditions, Q. J. Roy. Meteor. Soc., 128,
389 1095–1135, 2002.
- 390 Xie, S., Zhang, M., Branson, M., et al.: Simulations of midlatitude frontal clouds by single-
391 column and cloud-resolving models during the Atmospheric Radiation Measurement
392 March 2000 cloud intensive operational period, J. Geophys. Res., 110, D15S03,
393 doi:10.1029/2004JD005119, 2005.
- 394 Xie, S., Zhang, Y., Giangrande, S. E. , Jensen, M. P., McCoy, R. and Zhang, M.: Interactions
395 between cumulus convection and its environment as revealed by the MC3E sounding
396 array, J. Geophys. Res. Atmos., 119, 11,784–11,808, doi:10.1002/2014JD022011, 2014.
- 397 Xu, K.-M., Cederwall, R. T., Donner, L. J., Grabowski, W. W., et al.: An inter-comparison of
398 cloud-resolving models with the Atmospheric Radiation Measurement summer 1997
399 IOP data, Quart.J. Roy. Meteorol. Soc., 128, 593-624, 2002.
- 400 Xue, H., and Feingold, G.: Large-eddy simulations of trade wind cumuli: Investigation of
401 aerosol indirect effects, J. Atmos. Sci., 63, 1605–1622, doi:10.1175/JAS3706.1, 2006.
- 402

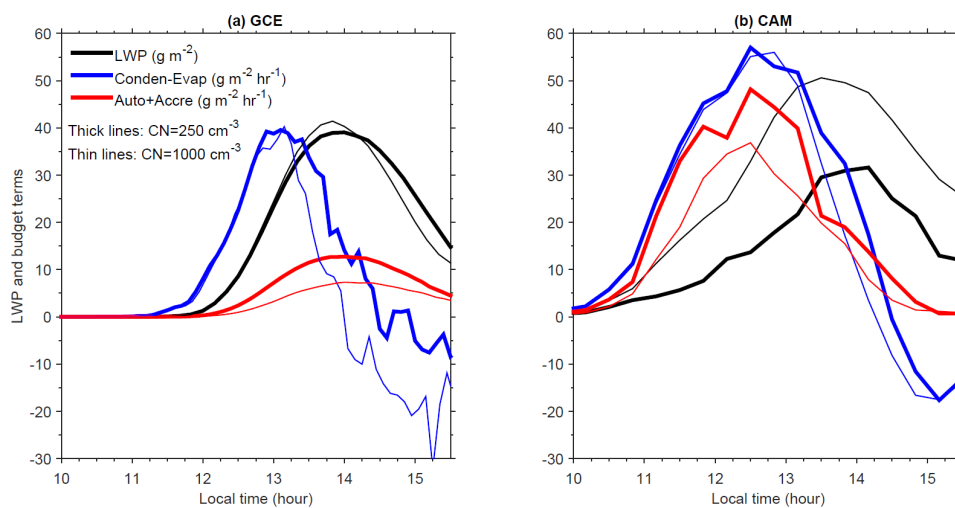


403
404
405
406
407
408

Figure 1. Observed cloud fractions on May 27th, 2011 at the SGP site (a); domain averaged cloud water content from the GCE model (b) and the single column version of CAM (c) for the case assuming a surface aerosol number of 500 cm⁻³; liquid water path and surface precipitation rates from GCE (d, f) and CAM (e, g) with varying surface aerosol number concentrations.

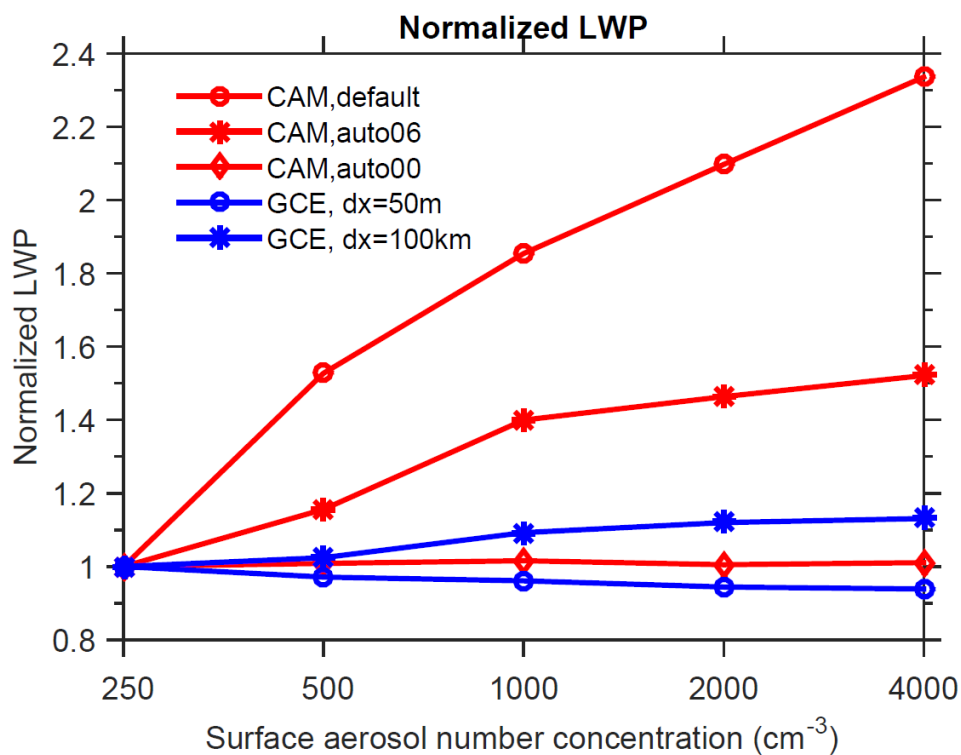


409
 410 **Figure 2.** (a-c) Domain averaged potential temperatures (θ), total water specific humidity
 411 (q_t) and cloud water content (q_c) at three times (13:00, 14:00 and 15:00) from two GCE
 412 cases with surface aerosol numbers equal to 250 cm^{-3} (dash-dotted curves) and 1000 cm^{-3}
 413 (solid curves). (d-f) Averaged profiles of q_c , net results of condensation and evaporation
 414 (Condensation-Evaporation), and (Condensation-Evaporation)/ q_c for the 1-hour interval from 13:00 to 14:00
 415 from the two CRM cases with surface aerosol numbers equal to 250 cm^{-3} (blue dash-dotted
 416 curves) and 1000 cm^{-3} (solid red curves). (g-i) Same as (d-f) except for the 1-hour interval
 417 from 14:00 to 15:00.



418
419
420
421
422
423

Figure 3. LWP and the column integrated LWP source and sink terms from the case with surface aerosol number concentration equal to 250 cm^{-3} (thick lines) and 1000 cm^{-3} (thin lines) for (a) GCE and (b) CAM.



424
425

Figure 4. Normalized LWP as a function of surface aerosol concentration in CAM (red curves) and GCE (blue curves). A case for CAM using an autoconversion rate proportional to $N_d^{-0.6}$ (CAM, auto06) as well as a case in which autoconversion is independent of N_d (CAM, auto00) is shown. The GCE model was run with a horizontal grid resolution of 50 m (default case) and 100 km.

431